Journal of Ovonic Research Vol. 19, No. 5, September - October 2023, p. 513 - 523

Investigation on the physical properties of Ni doped $SrTiO_3$ by first-principle calculations

M. M. Hameed[a], S. A. Aldaghfag[b,*], M. Saeed[a], M. Yaseen[a], S, Saleem[a], Nasarullah[a]
[a]*Spin-Optoelectronics and Ferro-Thermoelectric (SOFT) Materials and Devices Laboratory, Department of Physics, University of Agriculture, Faisalabad 38040, Pakistan*
[b]*Department of Physics, College of Sciences, Princess Nourah bint Abdulrahman University, P. O. Box 84428, Riyadh 11671, Saudi Arabia*

In present work, the magneto-electronic and optical features of $Sr_{1-x}Ni_xTiO_3$ (x = 12.5%, 25%, 50% and 75%) compounds are calculated using full potential linearized augmented plane wave (FP-LAPW) scheme within density functional theory (DFT) as employed in WIEN2k software. The electronic band structures (BS) and density of states (DOS) interpret the induced half metallic ferromagnetism mainly originating from highly spin polarized Ni-*d* states. The computed value of total magnetic moment of $Sr_{1-x}Ni_xTiO_3$ is 1.99998, 1.99991, 2.00003 and 2.00005 μB at 12.5%, 25%, 50% and 75% concentration respectively, which emerge primarily due to Ni-3*d* electrons. Furthermore, the optical features (refraction, dielectric function, absorption, and reflectivity) have also been computed within energy range of 0-10 eV. $Sr_{1-x}Ni_xTiO_3$ is optically active in visible to ultraviolet (UV) region owing to low reflectivity and high absorption. Results portray that the studied compound is a potential contender for its usage in the development of spintronic and optoelectronic devices.

(Received June 23, 2023; Accepted September 8, 2023)

Keywords: Ferromagnetic, Optical parameters, DFT, Spintronics

1. Introduction

A highly spin-polarized current is an important property of futuristic spintronic data storage devices, which plays key role in quantum probabilistic computing [1]. Half-metals (HM) are the only materials that can be used to achieve maximum degree of spin polarization [2]. Since the Fermi surfaces of these materials are completely spin-polarized, which act as metals in one spin direction and as insulators or semiconductors in the other [3]. To date, a few half-metals have been discovered, such as Heusler compounds, transition metal (TM) oxides including spinel, perovskite compounds, and TM doped dilute magnets [3-6]. Indeed, stable ferromagnetism along with 100% spin polarization (SP) above Fermi level (E_F) is sensitive to even minor details [7]. This makes a strong case to implement various engineering techniques to study the effect of minor magnetic substitutions in a host crystal to induce the magnetism in it. In this way, materials are obtained with desired magnetic properties for specific applications [8]. The technical and scientific significance of perovskites are explored because of their usages in solar cells, sensors, photovoltaic, spintronics and superconductors. Perovskite oxides exhibit a lot of exciting features such as ferromagnetism (FM) [9], piezoelectricity [10], electro-optics [11] etc., which further changed via doping of transition metals (TMs) and rare earth elements. The existence of TMs makes them useful materials for magneto-electricity [12], ferroelectricity [13], colossal magneto resistivity [14] based gadgets. In addition, the half metallic ferromagnetism (HMF) behavior has also been reported in these compounds owing to their exotic spin polarization. In 1983, HMF was first revealed while studying the SP of half-Heusler (NiMnSb) material [14]. Several TMs based

---

[*] Corresponding author: saaldaghfaq@pnu.edu.sa
https://doi.org/10.15251/JOR.2023.195.513

perovskite materials such as Cr doped $LaAlO_3$ [15], V/Co-doped $SrTiO_3$ [16, 17], iron-doped $SrTiO_3$ [18] and $BaTiO_3$ [19] etc. have been studied due to their HM features.

Specifically, strontium titanate (STO) belongs to the family of perovskite oxides having potential usage in various electro-optical devices [17]. It is anticipated as quantum ferroelectric or paraelectric oxide which attained significant attention due to its exceptional tenability via temperature and with applied electric field which results in its high dielectric constant with minimum loss [20]. STO is diamagnetic (zero magnetic moment) material and is transparent to visible light and shows absorbance in UV range. The inactivity of the material in visible range is owing to its wide E_g (indirect 3.25 eV) [21], so STO is required to be doped with TMs to tune the band gap (E_g). Doping of TMs can be an effective way to enhance the absorbance of visible light owing to 3*d*-TMs which form new energy levels within E_g and induce magnetism in STO that further can be used in spintronic devices [22-26]. According to experimental study, STO showed 3.25 (indirect) and 3.75 eV (direct) bandgap by utilizing the spectroscopic ellipsometry [21]. Maikhuri *et al.* investigated the doping of iron (at A and B site) in $BaTiO_3$ and revealed the increase in saturation magnetization by Fe doping at A-site while coercive field increased at B-site doping [27]. From theoretical point of view, Aboub *et al.* explored the effect of Ni doping (x=12.5%) in STO in which the E_g of doped compound abridged with improved structural stability [28]. Recently, our group published the formation energy, electronic, optical, and magnetic features of pure and V-doped STO computed by FP-LAPW scheme which confirmed semiconductive nature of pristine STO and HM nature of V doped STO [16]. Furthermore, the doping of Fe in STO also showed HMF behavior for A-site doping whereas metallic behavior with B-site substitution. In addition, at A-site doping, the material is prominent for application in spintronics devices [18].

In present study, the optoelectronic and magnetic characteristics of Ni doped $SrTiO_3$ are examined within FP-LAPW approach based on WIEN2k code [29]. Results exhibit that the $Sr_{1-x}Ni_xTiO_3$ compound demonstrates FM and suggests applications in spintronics, solar cells and other optical gadgets.

2. Method of calculation

DFT is a reliable and prominent computational tool which has been frequently used for the exploration of physical features of solid state systems. In WIEN2k software, the DFT based FP-LAPW approach is used to solve the Kohn-Sham equations [30]. In this approach, a simulated unit cell is distributed into two regions: interstitial region (plane wave like function) and the muffin tin region (atomic spheres with non-overlapping orbitals) as depicted by Fourier series [31, 32]. The parameters l_{max} = 10 (maximum angular momentum) and $R_{MT} \times K_{max} = 9$ (where R_{MT} is radii of muffin tin spheres and K_{max} denote the maximum K-vector in reciprocal space), respectively are considered. The R_{MT} values of Ni, Sr, Ti and O are 2.51, 2.47, 1.84 and 1.63 bohr, correspondingly. The electronic configurations of elements are Ni ($4s^2$, $3d^8$), Sr ($5s^2$), Ti ($4s^2$, $3d^2$), and O ($2s^2$, $2p^4$). The value of charge density Fourier expansion G_{max} = 12 is used for atomic radii conversion. In the first Brillouin Zone (BZ), the 1000 k-points are utilized for the energy convergence. In unit-cell, the cut-off energy value of -6.0 Ry was set to distinct the core and valance states. Self-consistency was considered at energy convergence near to 10^{-5} Ry.

3. Results and discussions

3.1. Electronic properties

The SP energy states dispersion can be studied by evaluation of BS and DOS including total DOS and partial DOS. BS and E_g of a semiconductor (SC) are vital parameters which predict the possibility of any materials application in magneto-optical and optoelectronic gadgets. The spin dependent BS of $Sr_{1-x}Ni_xTiO_3$ (x = 12.5%, 25%, 50% and 75%) are calculated along high symmetric BZ by using PBEsol + GGA approximation as depicted in Fig. 1(a-d).

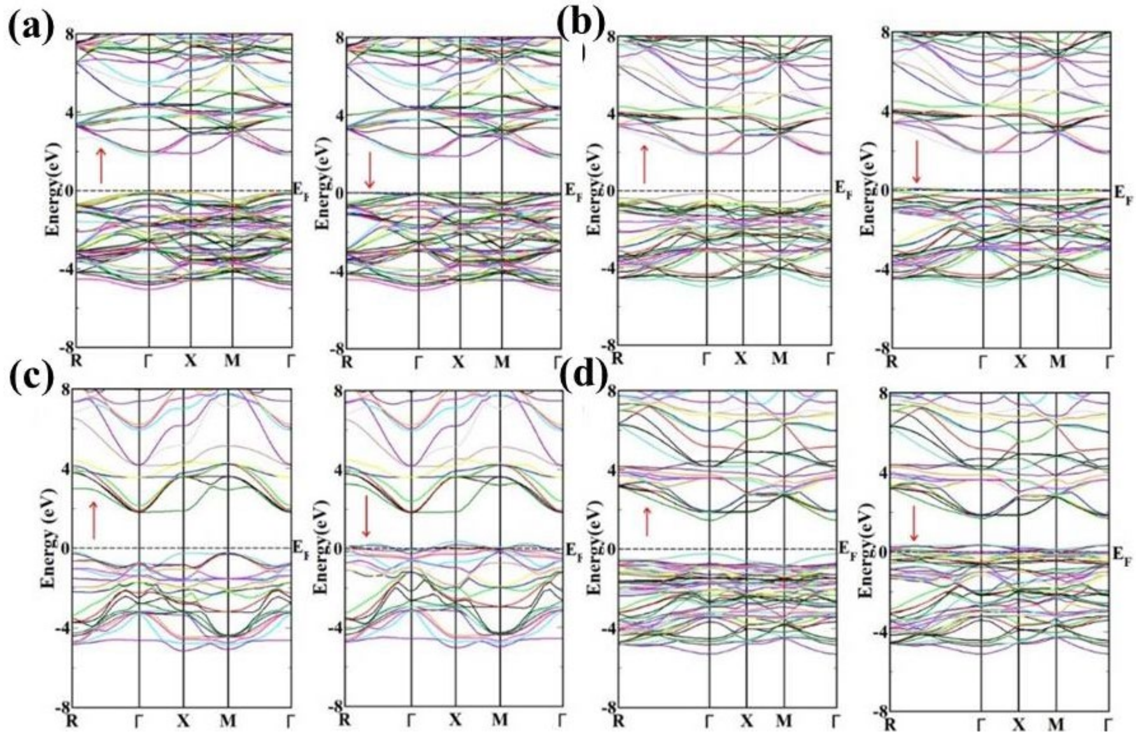

Fig. 1. Spin resolved BS of $Sr_{1-x}Ni_xTiO_3$ at (a) $Sr_{0.875}Ni_{0.1250}TiO_3$ *(b)* $Sr_{0.75}Ni_{0.25}TiO_3$ *(c)* $Sr_{0.5}Ni_{0.5}TiO_3$ *and (d)* $Sr_{0.25}Ni_{0.75}TiO_3$

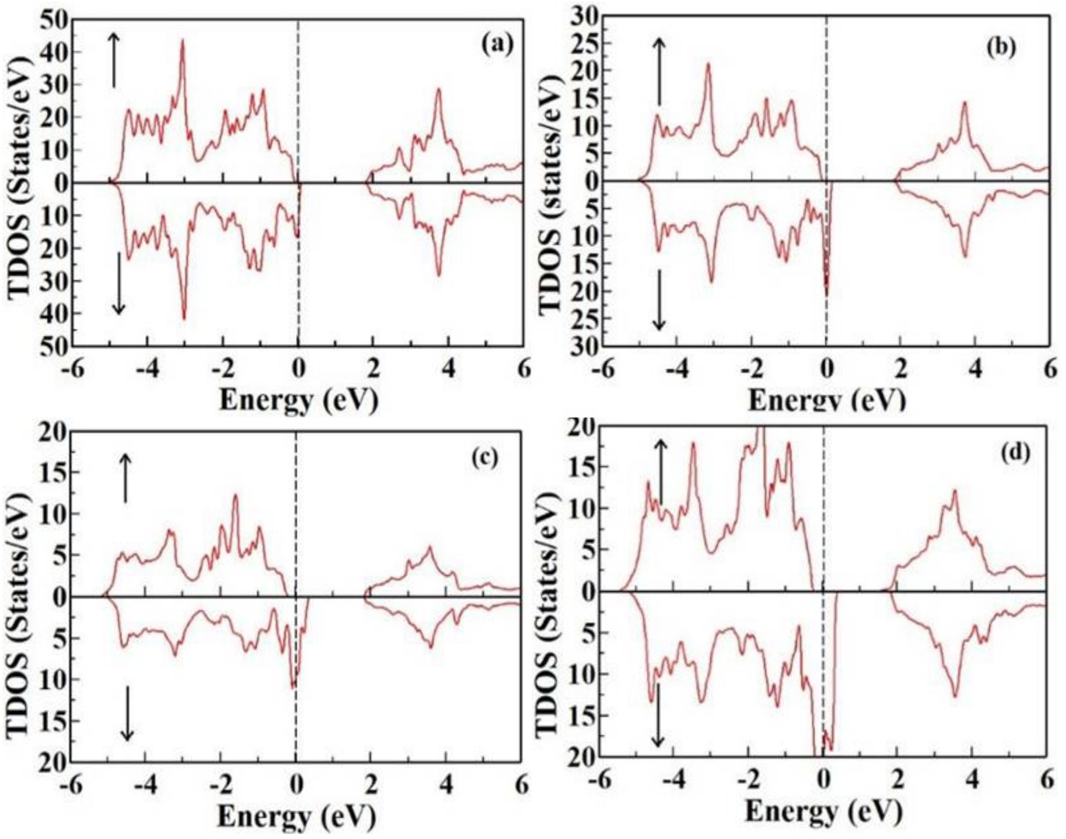

Fig. 2. TDOS plots of $Sr_{1-x}Ni_xTiO_3$ at (a) $Sr_{0.875}Ni_{0.1250}TiO_3$ *(b)* $Sr_{0.75}Ni_{0.25}TiO_3$, *(c)* $Sr_{0.5}Ni_{0.5}TiO_3$ *and (d)* $Sr_{0.25}Ni_{0.75}TiO_3$

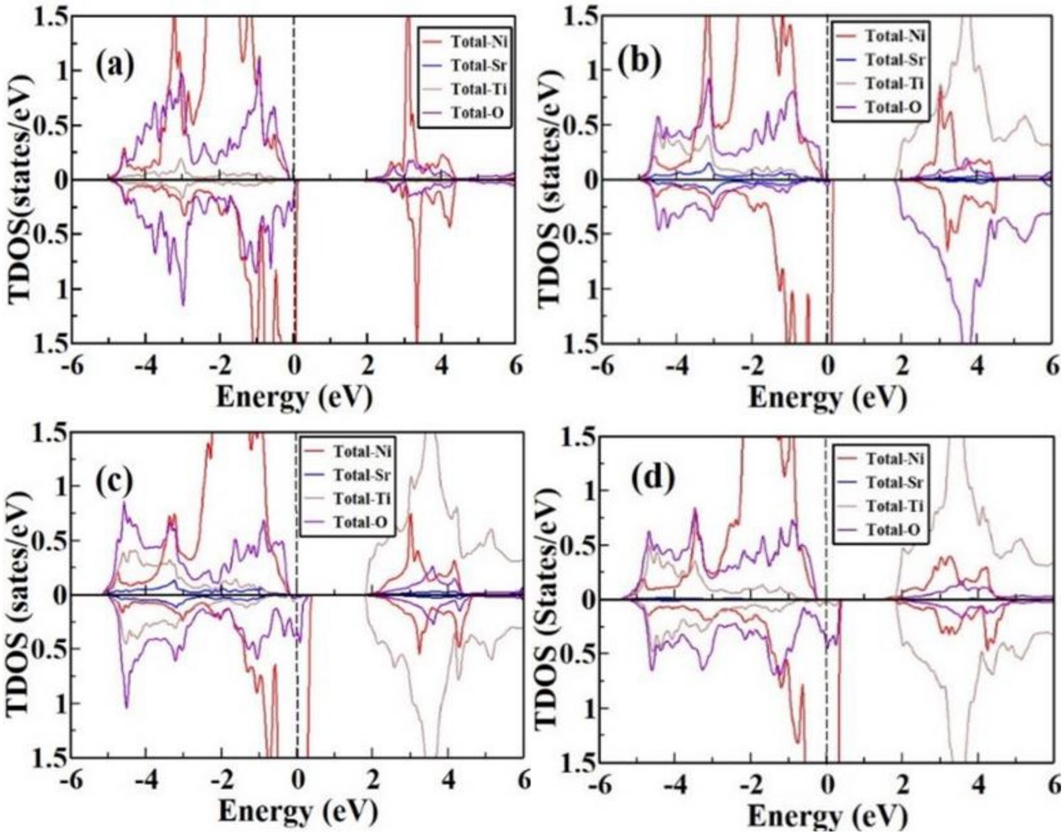

Fig. 3. Atomic TDOS plots of $Sr_{1-x}Ni_xTiO_3$ at (a) $Sr_{0.875}Ni_{0.1250}TiO_3$ *(b)* $Sr_{0.75}Ni_{0.25}TiO_3$*, (c)* $Sr_{0.5}Ni_{0.5}TiO_3$ *and (d)* $Sr_{0.25}Ni_{0.75}TiO_3$

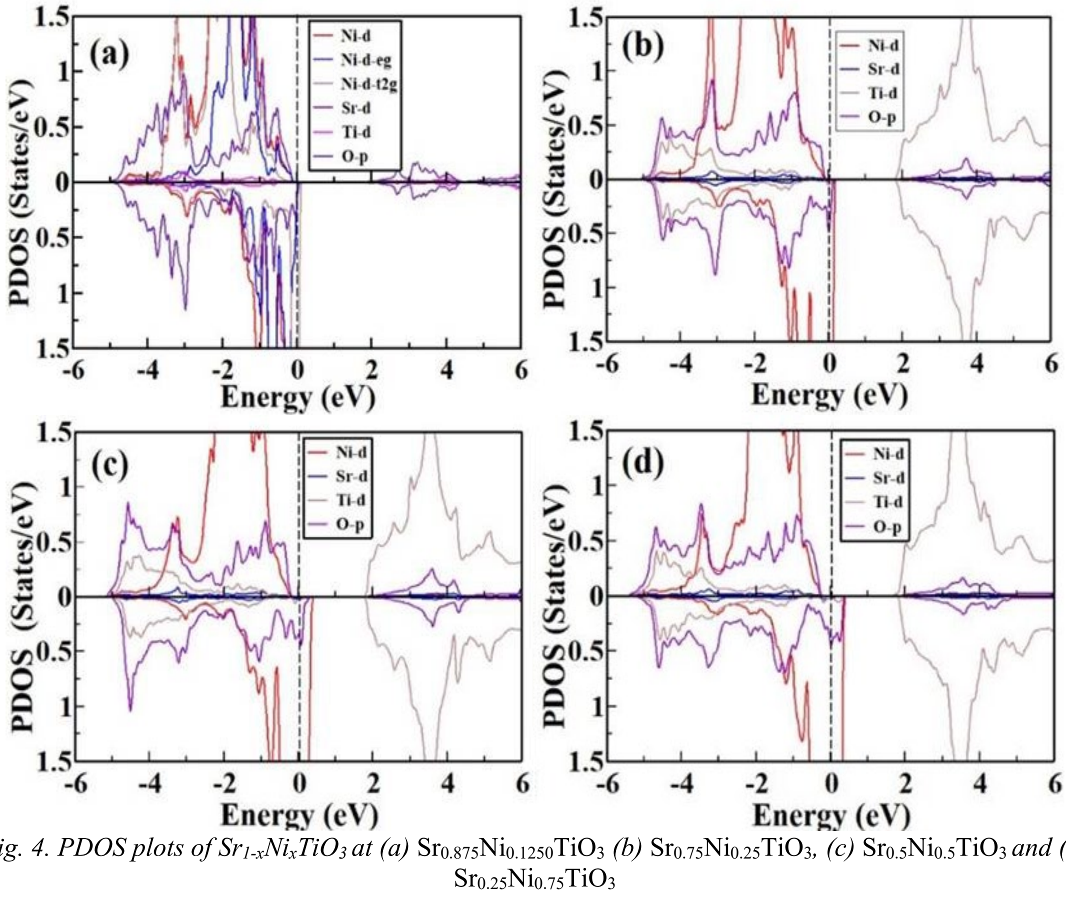

Fig. 4. PDOS plots of $Sr_{1-x}Ni_xTiO_3$ at (a) $Sr_{0.875}Ni_{0.1250}TiO_3$ *(b)* $Sr_{0.75}Ni_{0.25}TiO_3$*, (c)* $Sr_{0.5}Ni_{0.5}TiO_3$ *and (d)* $Sr_{0.25}Ni_{0.75}TiO_3$

In earlier theoretical study, we investigated pure STO revealing the SC (E_g=1.88 eV) behavior with GGA method[16]. Presented study reveals that after doping, the $Sr_{1-x}Ni_xTiO_3$ show polarization in spin-up and spin-dn versions. It shows HMF behavior, as spin-up version has semiconducting nature while spin-dn version illustrates the metallic behavior showing 100% spin polarization. The following formula is commonly used to compute spin-polarization in half metallic ferromagnetic (HMF) materials [33].

$$P = \frac{N^{\uparrow}(E_F)-N^{\downarrow}(E_F)}{N^{\uparrow}(E_F)+N^{\downarrow}(E_F)} \tag{1}$$

The computed values of HM gaps are 2.81, 2.80, 2.76 and 2.52 eV respectively, at x=12.5%, 25%, 50% and 75% doping concentrations, correspondingly (see Fig. 1(c, d)). The diversity of their E_g indicates prospective applications in spintronic gadgets. The computed BSs are further analyzed by computing the total and partial DOS. The DOS data exhibits the deeper depiction of electronic correlations in system and also tells us about the state's density per electron volt. Total DOS of $Sr_{1-x}Ni_xTiO_3$ compound (see Fig. 2 and 3) illustrate the HM behavior as earlier explained through the analysis of BS. Partial DOS spectrum is mainly contributed by Ni-3*d* states. At 12.5% doping, Ni-3*d* split into doubly degenerated e_g (non-bonding) and triply degenerated t_{2g} (bonding) states. In spin-up, the participation of d_{eg} states is large and small in d_{t2g} spin-splitting. While the d_{t2g} state contribution is large in dn-spin channel in the vicinity of E_F (see Fig. 4a). On the other hand, the O-2*p* states with feeble participation of Ti/Sr-*d* states for both spin versions are present in valance band (VB) and conduction band (CB) is found to be composed of primarily from O-2p state. However, there is a strong hybridization occurs between O-2*p* and Ni-3*d* orbits along E_F in spin-dn channel. Furthermore, at 25%, 50% and 75% doping, the major peaks in VB are owing to Ni/Ti-*d* and O-2*p* states. While in CB region, Ti-3*d* and O-2*p* states are dominant from 2-6 eV for boh spin version (see Fig. 4(b-d)). The hybridization is observed owing to Ni/Sr-*d* states at -4.8 eV.

3.2. Optical properties

Optical features can be studied by examining how light interacts with matter, specifically when valence electrons gain energy from incident light and make transition towards conduction band. The interband transitions are important for optical devices while intraband transitions do not contribute to optical conduction. Moreover, E_g is also a crucial factor due to its importance in defining the absorption edge [34-36]. The optical parameters of solid state system are determined by analyzing the complex dielectric function ε(ω) that can be expressed as [37-39].

$$\varepsilon\,(\omega) = \varepsilon 1\,(\omega) + i\varepsilon 2\,(\omega) \tag{2}$$

where $\varepsilon_1(\omega)$ corresponding to real part of the ε(ω) which is concerned with light polarization while $\varepsilon_2(\omega)$ portrays the absorption of impinging light. $\varepsilon_1(\omega)$ is linked to $\varepsilon_2(\omega)$ through Kramers-Krong expressions that can be computed as [40].

$$\varepsilon_1 = 1 + \frac{2}{\pi} P \int_0^{\infty} \frac{\varepsilon 2(\omega')\omega' d\omega'}{\omega'^2-\omega^2}\, d\omega' \tag{3}$$

where *P* is integral's principal value. The static dielectric constant $\varepsilon_1(0)$ is dependent on the E_g because at zero electron volt, there is no participation from the lattice. $\varepsilon_1(0)$ increase from 28.4 to 160.7 with increasing concentration of Ni. Various optical parameters at zero frequency are listed in Table 1. The inverse relation exists between $\varepsilon_1(0)$ and the E_g agreeing with Penn's model [41].

$$\varepsilon_1(0) = 1 + \left(\frac{\mathrm{h}\omega_p}{E_g}\right)^2 \tag{4}$$

So, the materials which have maximum value of $\varepsilon_1(0)$ possess low E_g. The $\varepsilon_1(\omega)$ spectra obtained negative values at 0.76 eV which corresponds to the metallic behavior. The negative

$\varepsilon_1(\omega)$ is due to the excitations of heavy effective mass (collectively) which is caused by the applied electric field [42]. The highest peaks appeared at 4.36 eV for all doping concentration then starts to decline with increasing energy and becomes constant after 5.87 eV (see Fig. 5a). The absorption of light in material is denoted by $\varepsilon_2(\omega)$ and is linked with material's BS [43]. At 75% concentration, the $\varepsilon_2(\omega)$ shows highest peak (at 0.04 eV) value where light dispersion is minimum and light absorption is greater. After that a fast decline observed in $\varepsilon_2(\omega)$ that is owing to Plasmonic oscillations [16]. Further $\varepsilon_2(\omega)$ upsurge via increase in photon energy and maximum $\varepsilon_2(\omega)$ peak is obtained within range of 3.8-4.7 eV (see Fig. 5b).

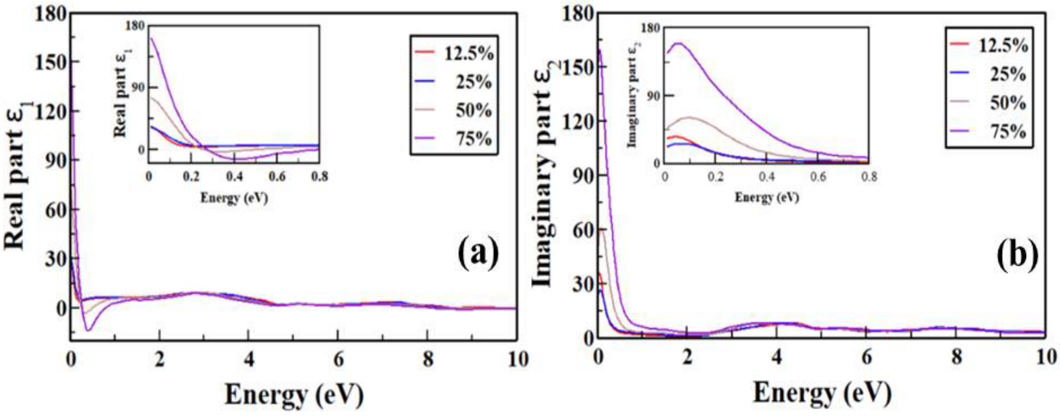

Fig. 5. (a) ε_1 (ω), (b) ε_2 (ω) plots of $Sr_{1-x}Ni_xTiO_3$

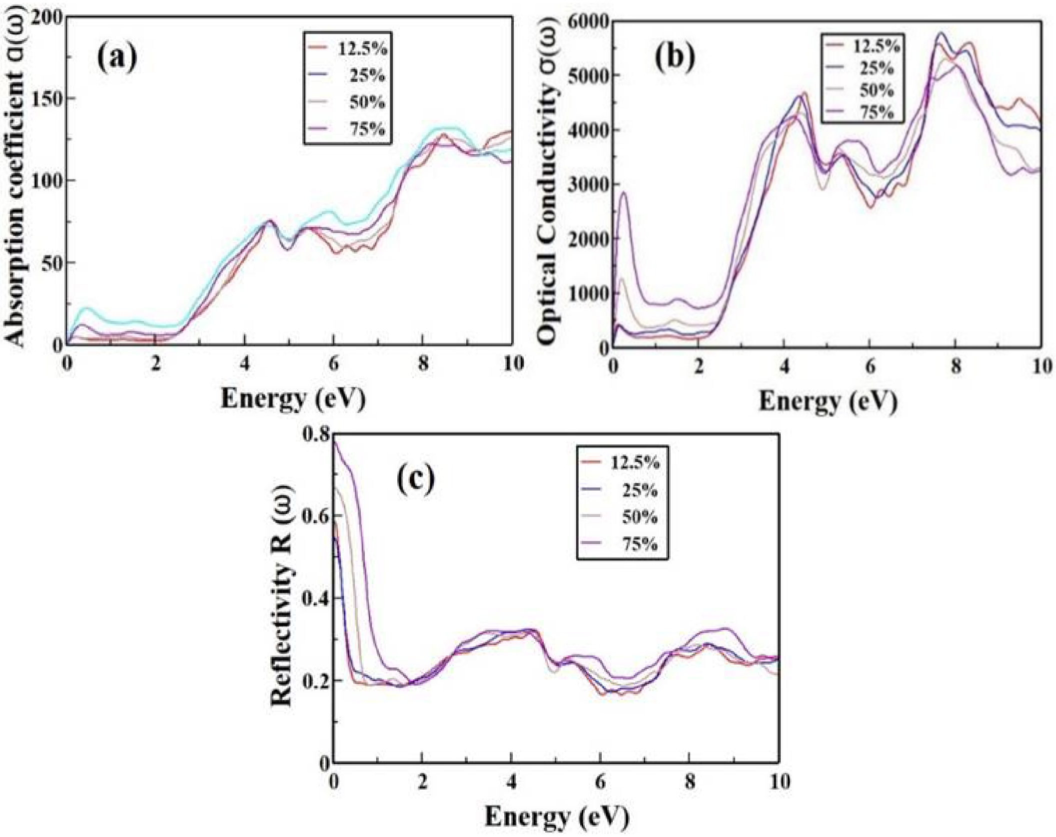

Fig. 6. (a) α (ω), (b) σ(ω) and (c) R (ω) plots of $Sr_{1-x}Ni_xTiO_3$

This change in energy span is primarily attributed owing to the dissimilarity in E_g at different doping concentration. The absorptive nature of the material is computed by computing the α(ω). The incident light has energy less than its threshold value, which corresponds to the E_g of the resultant material, cannot make electrons of VB to jump into CB [44]. It increases from threshold limit to reach a peak value (at 4.93 eV) in visible to ultraviolet (UV) region which discloses suitability of material for solar cell and optoelectronic devices (see Fig. 6a). By the following relation, absorption α(ω) and extinction coefficients k(ω) are linked to each other as follows [45].

$$k(\omega) = \frac{\alpha\lambda}{4\pi} \tag{5}$$

The free electrons transmit from VB to CB by gaining energy from incident light and further participate in conduction termed as optical conductivity σ(ω). It explains the bond breaking in studied compound owing to light absorption and it is directly related to absorption [46]. The σ(ω) starts from 0 eV, afterwards some attenuation (σ(ω)) with a value of 4120, 4656, 4333, 4222 $(\boldsymbol{\Omega}\text{cm})^{-1}$, for 12.5%, 25%, 50% and 75% doping, correspondingly (see Fig. 6b). The frequency-dependent reflectivity R(ω) is another optical parameter which reveals surface response to the incident energy and has an inverse relation with absorption [47]. R(ω) spectra is computed through following equations [48, 49].

$$R(\omega) = \frac{[n(\omega)-1]^2 + k^2(\omega)}{[n(\omega)+1]^2 + k^2(\omega)} \tag{6}$$

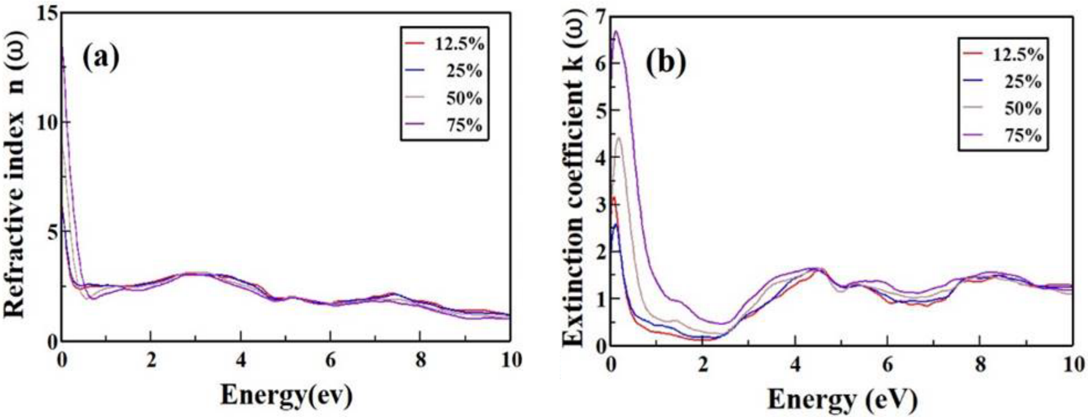

Fig. 7. (a) n (ω) and (b) k (ω) of plots of $Sr_{1-x}Ni_xTiO_3$.

Table 1. The premeditated Optical parameters at 0 eV for $Sr_{1-x}Ni_xTiO_3$

Optical Parameters At 0 eV	Doping Concentration of Ni-atom			
	x= 12.5%	x= 25%	x= 50%	x= 75%
ε_1 (0)	28.4	30.5	80.87	160.7
n (0)	14.1	7.42	12.63	6.81
R (0)	0.51	0.56	0.65	0.76

The static reflectivity R(0) is 0.51, 0.56, 0.65 and 0.76 for 12.5%, 25%, 50% and 75% doping, correspondingly (see Fig. 6c). With increasing photon frequency, its value starts to decrease via small bumps up to certain energy limit which linked to electronic (interband) transitions from VB to CB and maximum R(ω) is obtained at energy points of negative ε_1 (ω) values. To assess the suitability of a material for optical devices like solar cells and detectors, it is essential to determine its n(ω). The following formula is done for the calculation of n(ω) [50].

$$n(\omega) = \left(\frac{[\varepsilon_1^2\ (\omega) + \varepsilon_2^2\ (\omega)]^{\frac{1}{2}}}{2}\right)^{1/2} \tag{7}$$

At zero frequency, the estimated n(ω) for $Sr_{1-x}Ni_xTiO_3$ (x = 12.5%, 25%, 50% and 75%) is 14.1, 7.42, 12.63 and 6.81, respectively (see Fig. 7a). It upsurges with energy within visible range and decreases afterwards to its lowest value at higher energies. The highest peak of n(ω) lies within 3.1 - 3.9 eV. The attained results of ε_1 (0), n(0), R (0) are listed in Table 1. k(ω) discloses diminution of light (k > 0) that entering in material [51]. The ε_2 (ω) is linked via k(ω) through 2kn = ε_2 (ω). The maximum peaks of k(ω) appear at 4-4.8 eV energy range (see Fig. 7b). The optical outcomes indicate that the studied compound is suitable for optoelectronic gadgets.

3.3. Magnetic properties

Magnetic features are computed via spin-polarized computations. The moment (μ_B) values of Sr, Ti, O, Ni atoms, and total magnetic moment M_{Tot} of $Sr_{1-x}Ni_xTiO_3$ (x = 12.5, 25, 50 and 75%) are computed (see. Table 2). The individual magnetic moment of Ni, Sr, Ti and O are less than predicted M_{Tot} of Hund's rule [52] owing to the *p-d* exchange interaction. The M_{Tot} for 12.5%, 25%, 50% and 75% doping concentrations are 1.99998, 1.99991, 2.00003 and 2.00005 μ_B, respectively where the important role in M_{Tot} is due to Ni atom. Moreover, the sign of μ_B is used for spin configuration of each atom. The negative μ_B indicates ferrimagnetic and anti-FM behavior whereas positive μ_B is related to similar spin direction of electrons of different ions [53]. The μ_B of Sr and Ti favor anti parallel μ_B alignment and O favor parallel μ_B alignment.

Table 2. Calculated results of total, interstitial and individual atomic magnetic moment of each atom for $Sr_{1-x}Ni_xTiO_3$

	M_{int}	M_{Ni}	M_{Sr}	M_{Ti}	M_O	M_{Tot}
$Sr_{0.875}Ni_{0.1250}TiO_3$	0.02808	1.48864	-0.00068	-0.00408	0.03068	1.99998
$Sr_{0.75}Ni_{0.25}TiO_3$	0.02588	1.48794	-0.00016	-0.00866	0.04267	1.99991
$Sr_{0.5}Ni_{0.5}TiO_3$	0.01935	1.44892	-0.00029	-0.02106	0.08627	2.00003
$Sr_{0.25}Ni_{0.75}TiO_3$	0.01524	1.44763	-0.00015	-0.03124	0.09457	2.00005

4. Conclusions

The FP-LAPW scheme is employed to explore SP optoelectronic and magnetic characteristics of $Sr_{1-x}Ni_xTiO_3$ (x = 12.5%, 25%, 50% and 75%) compound. The HMF behavior of studied compound is confirmed by computing BS and DOS in which up-spin version exhibit semiconductive behavior and dn-spin version exhibit metallic nature. The contribution to M_{Tot} is mainly due to Ni-atom. Furthermore, $Sr_{1-x}Ni_xTiO_3$ (x = 12.5%, 25%, 50% and 75%) compound illustrate the M_{Tot} of 1.999, 1.999, 2.000, 2.000 μ_B, correspondingly. Optical properties are also explored within range of 0-10 eV. α (ω) and σ (ω) are highest in visible-UV span of light along with low R(ω). The outcomes signify that the explored material have possible usage in optoelectronic and magnetic devices.

Acknowledgements

This research project was funded by the Deanship of Scientific Research, Princess Nourah bint Abdulrahman University, through the Program of Research Project Funding After Publication, grant No (44- PRFA-P- 89)

References

[1] D. D. Awschalom , R. Epstein , R. Hanson, Scientific American, 297(4), 84-91 (2007); https://doi.org/10.1038/scientificamerican1007-84

[2] I. Galanakis, P. H. Dederichs, N. Papanikolaou. Physical Review B, 66(17), 174429 (2002); https://doi.org/10.1103/PhysRevB.66.174429

[3] A. Sohail, S. A. Aldaghfag, M. K. Butt, M. Zahid, M. Yaseen, J. Iqbal , M. Ishfaq , A. Dahshan, Journal of Ovonic Research 17(5), 461-469 (2021); https://doi.org/10.15251/JOR.2021.175.461

[4] M. Jourdan, J. Minár, J. Braun, A. Kronenberg, S. Chadov, B. Balke, A. Gloskovskii, M. Kolbe, H. J. Elmers, G. Schönhense, H. Ebert, Nature communications, 5(1), 3974 (2014); https://doi.org/10.1038/ncomms4974

[5] P. Mavropoulos, K. Sato, R. Zeller, P. H. Dederichs, V. Popescu, H. Ebert, Physical Review B, 69(5), 054424 (2004); https://doi.org/10.1103/PhysRevB.69.054424

[6] Z. Liu, S. Zhang, X. Wang, X. Ye, S. Qin, X. Shen, D. Lu, J. Dai, Y. Cao, K. Chen, F. Radu, Advanced Materials, 34(17), 2200626 (2022); https://doi.org/10.1002/adma.202200626

[7] S. Bhattacharya, R. Das, A. K. Kundu, M. M. Seikh, Journal of Magnetism and Magnetic Materials, 557, 169466 (2022); https://doi.org/10.1016/j.jmmm.2022.169466

[8] D. P. Arnold , N. Wang, Journal of microelectromechanical systems, 18(6), 1255-1266 (2009); https://doi.org/10.1109/JMEMS.2009.2034389

[9] T. Chiba, T. Atou, Y. Syono, J. Solid State Chem. 132, 139-143 (1997); https://doi.org/10.1006/jssc.1997.7432

[10] S. Zhang, R. Xia, T. R. Shrout, J. Appl. Phys. 100, 104108 (2006); https://doi.org/10.1063/1.2382348

[11] M. Crespin, W. K. Hall, J. Catal. 69, 359 (1981); https://doi.org/10.1016/0021-9517(81)90171-8

[12] B. B. V. Aken, T. T. M. Palstra, A. Filippetti, N. A. Spaldin, Nat. Matter 3, 164 (2004); https://doi.org/10.1038/nmat1080

[13] G. H. Haertling, J. Am. Ceram. Soc. 82, 797 (1999); https://doi.org/10.1111/j.1151-2916.1999.tb01840.x

[14] R. A. de Groot, F. M. Mueller, P. G. van Engen, K. H. J. Buschow, Phys. Rev. Lett. 50, 2024-2027 (1983); https://doi.org/10.1103/PhysRevLett.50.2024

[15] H. Javid, S. A. Aldaghfag, M. K. Butt, S. Mubashir, M. Yaseen, M. Ishfaq, S. Saleem, H. E. Alic, H. H. Hegazy, Journal of Ovonic Research, 18(4), 481-489 (2022); https://doi.org/10.15251/JOR.2022.184.481

[16] S. Saleem, S. A. Aldaghfag, M. Yaseen, M. K. Butt, M. Zahid, A. Murtaza, A. Laref, The European Physical Journal Plus, 137(1), 121 (2022); https://doi.org/10.1140/epjp/s13360-022-02352-z

[17] M. Ishfaq, M. Yaseen, F. F. Al-Harbi, M. K. Butt, Physica B: Condensed Matter, 664, 415025 (2023); https://doi.org/10.1016/j.physb.2023.415025

[18] H. Shafique, S. A. Aldaghfag, M. Kashif, M. Zahid, M. Yaseen, J. Iqbal , R. Neffati, Chalcogenide Letters, 18(10), 589 - 599 (2021); https://doi.org/10.15251/CL.2021.1810.589

[19] P. S. Sengunthar, R. J. Pandya, U. S. Joshi, AIP Conference Proceedings 1837(1), 040017 (2017); https://doi.org/10.1063/1.4982101

[20] F. W. Lytle, J. Appl. Phys. 35(7) 2212-2215 (1964); https://doi.org/10.1063/1.1702820

[21] Van Benthem, C. Elsser, R. H. French, J. Appl. Phys. 90, 6156 (2001); https://doi.org/10.1063/1.1415766
[22] J. Liu, G. Chen, Z. Li, Z. Zhang, J. Solid State Chem. 179, 3704 (2006); https://doi.org/10.1016/j.jssc.2006.08.014
[23] F. Li, K. Yu, L.-L. Lou, Z. Su, S. Liu, Mater. Sci. Eng., B 172, 136 (2010); https://doi.org/10.1016/j.mseb.2010.04.036
[24] R. Niishiro, H. Kato, A. Kudo, Phys. Chem. Chem. Phys. 7, 2241 (2005); https://doi.org/10.1039/b502147b
[25] H. -C. Chen, C. -W. Huang, J. C. S. Wu, S. -T. Lin, J. Phys. Chem. C 116, 7897 (2012); https://doi.org/10.1021/jp300910e
[26] X. Zhou, J. Shi, C. Li, J. Phys. Chem. C 115, 8305 (2011); https://doi.org/10.1021/jp200022x
[27] N. Maikhuri, A. K. Panwar, A. K. Jha, Journal of Applied Physics 113, 17D915 (2013); https://doi.org/10.1063/1.4796193
[28] Z. Aboub, B. Daoudi, A. Boukraa, AIMS Materials Science, 7(6), 902-910 (2020); https://doi.org/10.3934/matersci.2020.6.902
[29] M. Yaseen, A. Ashfaq, A. Akhtar, R. Asghar, H. Ambreen, M. K. Butt, S. Noreen, S. U. Rehman, S. Bibi, S. M. Ramay, A. Murtaza, Materials Research Express, 7(1), 015907 (2020); https://doi.org/10.1088/2053-1591/ab6110
[30] S. A. Aldaghfag, A. Aziz, A. Younas, M. Yaseen, A. Murtaza, H. H. Hegazy, Journal of Solid State Chemistry, 312, 123179 (2022); https://doi.org/10.1016/j.jssc.2022.123179
[31] Z. Ali, I. Khan, I. Ahmad, M. S. Khan, S.J. Asadabadi, Mater. Chem. Phys. 162, 308-315 (2015); https://doi.org/10.1016/j.matchemphys.2015.05.072
[32] G. Murtaza, N. Yousaf, A. Laref, M. Yaseen, Z. Naturforsch 73(4), 285-293 (2018); https://doi.org/10.1515/zna-2017-0388
[33] R. J. Soulen, J. M. Byers, M. S. Osofsky, B. Nadgorny, T. Ambrose, S. F. Cheng, A. Barry, Sci. 282(5386), 85-88 (1998); https://doi.org/10.1126/science.282.5386.85
[34] A. M. E. Raj, G. Selvan, C. Ravidhas, M. Jayachandran, C. Sanjeeviraj, J. Colloid Interface Sci. 328, 396-401 (2008); https://doi.org/10.1016/j.jcis.2008.08.052
[35] Q. Mahmood, M. Hassan, S. H. A. Ahmad, K. C. Bhamu, S. M. Ramay, J. Phys. Chem. Solid. 128, 283-290 (2019); https://doi.org/10.1016/j.jpcs.2017.08.007
[36] F. Zerarga, A. Bouhemadou, R. Khenata, S. Bin-Omran, Solid State Sci. 13, 1638-1648 (2011); https://doi.org/10.1016/j.solidstatesciences.2011.06.016
[37] S. Touam, R. Belghit, R. Mahdjoubi, Y. Megdoud, H. Meradji, M. S. Khan , R. Ahmed , R. Khenata , S. Ghemid , D. P. Rai , Y. Al-Douri, Bull. Mater. Sci. 43, 22 (2020); https://doi.org/10.1007/s12034-019-1978-y
[38] Y. Al-Douri, M. Ameri, A. Bouhemadou, K. M. Batoo, Phys. Status Solidi Basic Res. 256(11), 1900131 (2019); https://doi.org/10.1002/pssb.201900131
[39] H. Absike, N. Baaalla, L. Attou, H. Labrim, B. Hartiti, H. Ez-zahraouy, Solid State Commun. 3, 114684 (2022); https://doi.org/10.1016/j.ssc.2022.114684
[40] M. Rashid, Q. Mahmood, M. Hassan, M. Yaseen, A. Laref, Phys. Scripta 94(12), 125709 (2019); https://doi.org/10.1088/1402-4896/ab154f
[41] S. Wemple, M. DiDomenico Jr., Phys. Rev. B 3, 1338 (1971); https://doi.org/10.1103/PhysRevB.3.1338
[42] G. Marius, Kramers-Kronig relations, in: The Physics of Semiconductors, Springer, Berlin Heidelberg, 2010; https://doi.org/10.1007/978-3-642-13884-3_26
[43] A. M. Shawahni, M. S. Abu-Jafar, R. T. Jaradat, T. Ouahrani, R. Khenata, A. A. Mousa , K. F. Ilaiwi, Materials 11(10), 2057 (2018); https://doi.org/10.3390/ma11102057

[44] M. A. Khan, H. A. Alburaih, N. A. Noor, A. Dahshan, Solar Energy, 225, 122-128 (2021); https://doi.org/10.1016/j.solener.2021.07.026

[45] A. Aziz, S. A. Aldaghfag, M. Zahid, J. Iqbal, M. Yaseen , H. H. Somaily, Physica B: Condensed Matter, 630, 413694 (2022); https://doi.org/10.1016/j.physb.2022.413694

[46] F. Aslam, H. Ullah, M. Hassan, Materials Science and Engineering: B, 274, 115456 (2021); https://doi.org/10.1016/j.mseb.2021.115456

[47] I. Tariq, M. Yaseen, S. A. Aldaghfag, A. Aziz, Journal of Solid State Chemistry, 320, 123846 (2023); https://doi.org/10.1016/j.jssc.2023.123846

[48] R. Chen, D. Chen, W. Zhang, Results Phys. 30, 104864 (2021); https://doi.org/10.1016/j.rinp.2021.104864

[49] M. H. Benkabou, M. Harmel, A. Haddou, A. Yakoubi, N. Baki, R. Ahmed, Y. AlDouri, S. V. Syrotyuk, H. Khachai, R. Khenata, C. H. Voon, M. R. Johan, Chin. J. Phys. 56, 131-144 (2018); https://doi.org/10.1016/j.cjph.2017.12.008

[50] A. Bibi, I. Lee, Y. Nah, O. Allam, H. Kim, L. N. Quan, D. H. Kim, Mater. Today 49, 123-144 (2021); https://doi.org/10.1016/j.mattod.2020.11.026

[51] M. A. Khan, H. A. Alburaih, N. A. Noor, A. Dahshan, Solar Energy, 225, 122-128 (2021); https://doi.org/10.1016/j.solener.2021.07.026

[52] G. Murtaza, R. Khenata, S. Muhammad, A. H. Reshak, K. M. Wong, S. B. Omran, Z. A. Alahmed, Comput. Mater. Sci. 85, 402 (2014); https://doi.org/10.1016/j.commatsci.2013.12.054

[53] M. Nazar, S. A. Aldaghfag, M. Yaseen, M. Ishfaq, R. A. Khera, S. Noreen, M. H. Abdellattif, Journal of Physics and Chemistry of Solids, 166, 110719 (2022); https://doi.org/10.1016/j.jpcs.2022.110719